

# Subspace tracking for online system identification

Andr as Sasfi, Alberto Padoan, *Member, IEEE*, Ivan Markovsky, *Associate Member, IEEE*, Florian D orfler, *Senior Member, IEEE*

**Abstract**—This paper introduces an online approach for identifying time-varying subspaces defined by linear dynamical systems, leveraging optimization on the Grassmannian manifold leading to the *Grassmannian Recursive Algorithm for Tracking (GREAT)* method. The approach of representing linear systems by non-parametric subspace models has received significant interest in the field of data-driven control recently. We view subspaces as points on the Grassmannian manifold, and therefore, tracking is achieved by performing optimization on the manifold. At each time step, a single measurement from the current subspace corrupted by a bounded error is available. The subspace estimate is updated online using Grassmannian gradient descent on a cost function incorporating a window of the most recent data. Under suitable assumptions on the signal-to-noise ratio of the online data and the subspace’s rate of change, we establish theoretical guarantees for the resulting algorithm. More specifically, we prove an exponential convergence rate and provide a consistent uncertainty quantification of the estimates in terms of an upper bound on their distance to the true subspace. The applicability of the proposed algorithm is demonstrated by means of numerical examples, and it is shown to compare favorably with competing parametric system identification methods.

**Index Terms**—System identification, time-varying systems, subspace methods, behavioral systems, manifold optimization

## I. INTRODUCTION

Subspace representations of linear dynamical systems have recently attracted considerable attention in the control and system identification communities [1]–[8]. Rooted in behavioral systems theory [9], these representations offer a non-parametric framework that describes linear systems as subspaces containing all finite-horizon trajectories. Unlike traditional parametric models, this approach enables the identification of Linear Time-Invariant (LTI) behaviors directly from data that is sufficiently informative [5], [10]. The rise of this framework has spurred the development of subspace system identification methods [11] and novel data-driven control techniques [1]–[8]. These approaches exploit the subspace representation of a system, typically defined by the span of

a data matrix. Empirical studies have shown that they often outperform conventional parametric methods, providing robust and scalable solutions for modeling and control [12].

However, the applicability of these identification and control methods is limited to time-invariant systems. Recent surveys [13], [14] emphasize this research gap and highlight the challenge of online adaptation. Another open research challenge is the extension of data-driven control methods to nonlinear systems. Recent data-driven control methods exploit the fact that nonlinear systems can be over-approximated as Linear Time-Varying (LTV) systems under suitable assumptions on the time-variance [15], [16]. We adopt the perspective that trajectories of an LTV system always lie in a subspace that may change over time. Online identification of this non-parametric representation reduces to tracking this subspace. In this work, we address these challenges by proposing an algorithm that is capable of identifying the subspace representation of LTV systems online, with theoretical guarantees on the convergence rate and bias of the estimates.

Subspace tracking methods are used extensively in the field of signal processing [17]–[24], with a wide range of applications [18], [19]. Various frameworks have been developed based on, e.g., incremental singular value decomposition [20], recursive least squares method [21] or the Grassmannian optimization [22]–[24]. For some of these algorithms, theoretical guarantees have been derived, see [25] for a detailed summary. Most of them are asymptotic, but finite-sample guarantees also exist in the literature [26], [27]. Given the literature’s focus on signal processing, an important objective of the available subspace tracking methods is compressing large amounts of data. Therefore, the dimension of the considered subspace is typically much smaller than that of the embedding space, and the available algorithms exploit this property. However, this condition does typically not hold for linear dynamical systems with inputs [5]. Moreover, existing methods rely on assumptions of independence among samples, which do not hold in the case of dynamical systems where time series are inherently correlated. Thus, these methods are inherently unsuitable for online system identification.

To address these issues, we adopt a geometric approach and view subspaces as points on the Grassmannian manifold. Tracking can be posed as an unconstrained optimization problem on the manifold [28]–[30]. Techniques to solve unconstrained problems, such as gradient descent, are well-understood [29], [31] and allow for a simple analysis. This fact can be exploited to provide deterministic guarantees even

A. Sasfi, A. Padoan, and F. D orfler are with the Department of Information Technology and Electrical Engineering, ETH Z urich, 8092 Z urich, Switzerland (e-mail: {sasfi, apadoan, doerfler}@control.ee.ethz.ch).

I. Markovsky is with the Catalan Institution for Research and Advanced Studies, 08010 Barcelona, Spain, and also with the International Centre for Numerical Methods in Engineering, 08034 Barcelona, Spain (e-mail: ivan.markovsky@cimne.upc.edu).

in case the data are correlated, generated by linear dynamical systems, and subject to noise. Contrary to parametric system identification methods, we optimize a subspace which is a non-parametric model that uniquely defines the dynamical system. This model is coordinate-free, as it is independent of a basis. By optimizing the subspace directly (instead of a basis), we also alleviate the issue of non-convex orthogonality constraints.

The contributions of our work are the following. We propose a recursive algorithm for subspace tracking that is suitable for online identification of LTV systems from data corrupted by bounded measurement error. The method minimizes the projection error of an online data window onto the estimated subspace through gradient descent performed on the Grassmannian manifold. Assuming that the subspace's rate of change is bounded, we provide finite-sample convergence certificates for the algorithm, in the form of guaranteed convergence rate and bias. The derived bound explicitly depends on the subspace's rate of change, the bound on the measurement error, and the persistency of excitation property of the online data. In the special case of LTI systems and exact measurements, the derived bound is consistent, that is, the estimates converge to the true subspace exponentially fast.

The applicability of the proposed method is demonstrated on a numerical example, in which an LTV airplane model is identified from noisy data. We illustrate the predictive performance of the model obtained by our algorithm compared to two popular system identification methods. First, we show that the proposed algorithm outperforms the well-known offline subspace identification method N4SID [32] due to its capability of online adaptation. Second, we benchmark it against a standard online identification method, that estimates a parametric model via the recursive least squares technique [33]. While the two methods achieve similar prediction error nominally, the proposed gradient-based method exhibits better robustness properties against large measurement errors. Finally, we also study the conservatism of the theoretical bounds on a synthetic example.

The remainder of the paper is organized as follows. In Section II, we introduce the notation and provide preliminaries on subspaces and manifold optimization. We formulate the problem and motivate it through online system identification in Section III. The subspace tracking algorithm with the corresponding theoretical analysis is presented in Section IV. Section V contains the numerical examples, and Section VI concludes the paper. Most proofs are deferred to the Appendix.

## II. PRELIMINARIES

In this section, we introduce notation and differential-geometric concepts that are used later in the paper.

### A. Notation

Let  $\mathbb{N}$  ( $\mathbb{R}$ ) denote the set of positive integers (real numbers), and  $\mathbb{Z}_{\geq T}$  ( $\mathbb{R}_{\geq T}$ ) is the set of integers (real numbers) greater than or equal to  $T$ . We denote the trace of a square matrix  $A$  by  $\text{tr}(A)$ . Given two matrices  $A$  and  $B$ ,  $\langle A, B \rangle_F = \text{tr}(A^\top B)$  denotes the Frobenius inner product, and  $\|A\|_F$  is

the Frobenius norm of  $A$ . The  $i$ -th largest singular value of a matrix  $A$  is denoted by  $\sigma_i(A)$ . The identity matrix of size  $n \times n$  is  $I_n$ , and  $\text{diag}(d_1, d_2, \dots, d_n)$  denotes a diagonal matrix, with elements  $d_1, d_2, \dots, d_n$  on the main diagonal. The  $\ell_\infty$  norm of a sequence  $\{f_t\}_{t \geq T}$  is defined as  $\|f\|_\infty = \sup_{t \geq T} |f(t)|$ . By  $\mathcal{K}_\infty$  we denote the class of functions  $g : \mathbb{R}_{\geq 0} \rightarrow \mathbb{R}_{\geq 0}$  that are continuous, strictly increasing, and satisfy  $g(0) = 0$  and  $\lim_{r \rightarrow \infty} g(r) = \infty$ .

### B. Subspaces

Consider a subspace  $\mathbf{U}$  of dimension  $d$  in  $\mathbb{R}^n$  and matrix  $U \in \mathbb{R}^{n \times d}$  with  $U^\top U = I_d$  that represents the subspace, i.e.,  $\mathbf{U}$  is the image of  $U$ . The orthogonal projection onto  $\mathbf{U}$  and the orthogonal complement of  $\mathbf{U}$  are defined as  $P_{\mathbf{U}} = UU^\top$  and  $P_{\mathbf{U}}^\perp = I_n - P_{\mathbf{U}}$ , respectively. Note that the projections are independent of the subspace representation  $U$ , provided that  $U^\top U = I_d$  holds. We use the following properties of the projection matrices later on:  $P_{\mathbf{U}} = P_{\mathbf{U}}^\top = P_{\mathbf{U}}^2$  and  $\|P_{\mathbf{U}} M\| \leq \|M\|$  for any matrix  $M$  and any matrix norm  $\|\cdot\|$  [34], [35].

Now consider another subspace  $\mathbf{V}$  of the same dimension as  $\mathbf{U}$ , with representation  $V \in \mathbb{R}^{n \times d}$ ,  $V^\top V = I_d$ . The principal angles between  $\mathbf{U}$  and  $\mathbf{V}$  are denoted by  $0 \leq \theta_1 \leq \dots \leq \theta_d \leq \pi/2$ , and can be computed using, e.g., singular value decomposition (SVD), see [34, Sec. 6.4.3] for details. The following metrics will be used to quantify the distance between two subspaces [28], [30], [36], [37]

$$\text{Chordal: } d_2(\mathbf{U}, \mathbf{V}) = \left( \sum_{i=1}^d \sin^2 \theta_i \right)^{1/2} = (\text{tr}(P_{\mathbf{U}}^\perp P_{\mathbf{V}}))^{1/2},$$

$$\text{Gap: } d_\infty(\mathbf{U}, \mathbf{V}) = \sin \theta_d = \|P_{\mathbf{U}} - P_{\mathbf{V}}\|_2.$$

The inequality  $d_\infty(\mathbf{U}, \mathbf{V}) \leq d_2(\mathbf{U}, \mathbf{V}) \leq d \cdot d_\infty(\mathbf{U}, \mathbf{V})$  follows from the definition of the metrics immediately. Furthermore, the following property of the gap metric is useful.

*Lemma 1:* For any subspaces  $\mathbf{U}, \mathbf{V}$  of dimension  $d$  in  $\mathbb{R}^n$  and any  $u \in \mathbf{U}$ , the following relation holds

$$\|P_{\mathbf{V}}^\perp u\|_2 \leq d_\infty(\mathbf{U}, \mathbf{V}) \cdot \|u\|_2.$$

*Proof:*

$$\|(I_n - P_{\mathbf{V}})u\|_2 = \|(P_{\mathbf{U}} - P_{\mathbf{V}})u\|_2 \leq \|P_{\mathbf{U}} - P_{\mathbf{V}}\|_2 \|u\|_2. \quad \blacksquare$$

### C. Grassmannian geometry

This section introduces some concepts related to the *Grassmannian manifold* that are used throughout the paper. Formal definitions are outside of the scope of this paper, and the interested reader is referred to [29] for a thorough exposition. Informally, the Grassmannian manifold is the set of all subspaces in  $\mathbb{R}^n$  of a given dimension  $d$ :

$$\text{Gr}(n, d) = \{\text{subspaces of dimension } d \text{ in } \mathbb{R}^n\}.$$

The tangent space associated to each point on the manifold  $\mathbf{U} \in \text{Gr}(n, d)$  is denoted by  $T_{\mathbf{U}} \text{Gr}(n, d)$  (see [29, Def. 8.33] for a formal definition). The tangent bundle of a manifold is

the disjoint union of its tangent spaces, endowed with a smooth manifold structure, defined as

$$T\text{Gr}(n, d) = \{(\mathbf{U}, \mathbf{V}) \mid \mathbf{U} \in \text{Gr}(n, d), \mathbf{V} \in T_{\mathbf{U}}\text{Gr}(n, d)\}.$$

Points on the Grassmannian manifold are abstract objects. For computation purposes, we represent a point on  $\text{Gr}(n, d)$  by a matrix in  $\mathbb{R}^{n \times d}$ , whose columns are orthonormal and span the corresponding subspace<sup>1</sup>. Furthermore, for any representation  $U \in \mathbb{R}^{n \times d}$ ,  $U^T U = I_d$  of a point  $\mathbf{U} \in \text{Gr}(n, d)$ , all tangent vectors  $\mathbf{V} \in T_{\mathbf{U}}\text{Gr}(n, d)$  admit a representation  $V \in \mathbb{R}^{n \times d}$  that satisfies  $U^T V = 0$  [29]. In the following, we denote points on  $\text{Gr}(n, d)$  and  $T_{\mathbf{U}}\text{Gr}(n, d)$  by bold capital letters such as  $\mathbf{U}$  and  $\mathbf{V}$ . Any matrices  $U \in \mathbb{R}^{n \times d}$ ,  $U^T U = I_d$  and  $V \in \mathbb{R}^{n \times d}$  that represent  $\mathbf{U} \in \text{Gr}(n, d)$  and  $\mathbf{V} \in T_{\mathbf{U}}\text{Gr}(n, d)$  are denoted by capital letters in regular font.

The Grassmannian manifold can be equipped with a Riemannian metric using the Frobenius inner product making it a Riemannian manifold<sup>2</sup>. Given a differentiable function  $f$  that maps from  $\text{Gr}(n, d)$  to  $\mathbb{R}$ , the Riemannian gradient of  $f$  denoted by  $\text{grad } f$  is a vector field on the manifold. The gradient associates a point  $\mathbf{U} \in \text{Gr}(n, d)$  with a tangent vector  $\mathbf{V} \in T_{\mathbf{U}}\text{Gr}(n, d)$ , i.e.,  $\mathbf{V} = \text{grad } f(\mathbf{U})$ . A representation of  $\mathbf{V}$  can be calculated as [29, Sec. 9.16]

$$V = P_{\mathbf{U}}^{\perp} \nabla f(\mathbf{U}), \quad (1)$$

where  $\nabla f(\mathbf{U})$  is the Euclidean gradient of  $f$  evaluated at  $\mathbf{U}$ .

In manifold optimization, various maps (called retractions) are used to move along the manifold in the tangent directions. In this work, we use the *exponential map* due to its desirable theoretical properties. The exponential map maps an element of the tangent bundle  $(\mathbf{U}, \mathbf{V}) \in T\text{Gr}(n, d)$  to another element of the manifold  $\mathbf{U}^+ \in \text{Gr}(n, d)$ , i.e.,  $\mathbf{U}^+ = \text{Exp}_{\mathbf{U}}(\mathbf{V})$ . Consider a representation  $(U, V)$  of  $(\mathbf{U}, \mathbf{V})$ , and let  $V = Q_1 S Q_2$  denote the compact SVD, where  $S, Q_2 \in \mathbb{R}^{d \times d}$  and  $Q_1 \in \mathbb{R}^{n \times d}$  only contains columns corresponding to the non-zero singular values. Then, a representation of  $\mathbf{U}^+$  can be computed using the formula [28, Eq. (2.65)]

$$U^+ = [U Q_2 \ Q_1] \begin{bmatrix} \cos(S) \\ \sin(S) \end{bmatrix} Q_2^{\top}.$$

In the remainder of the paper, with a slight abuse of notation, we provide formulas for points in  $\text{Gr}(n, d)$  and  $T_{\mathbf{U}}\text{Gr}(n, d)$  using an arbitrary orthonormal matrix representation of them. However, this does not undermine consistency, since the quantities we work with, such as distances or projections, are coordinate-free notions defined for subspaces, not their representations. Consequently, these quantities are invariant under the choice of representation.

<sup>1</sup>In fact, the set  $\{U \in \mathbb{R}^{n \times d} \mid U^T U = I_d\}$  endowed with a differentiable structure is called the Stiefel manifold, and it is an embedded submanifold of the linear space  $\mathbb{R}^{n \times d}$ . The Grassmannian can be viewed as a quotient manifold of the Stiefel manifold. More details about quotient manifolds and the Grassmannian can be found in [29, Chp. 9].

<sup>2</sup>More precisely, the Frobenius inner product defines a Riemannian metric on the Stiefel manifold, which induces a Riemannian metric on the Grassmannian manifold [29, Sec. 9.7].

### III. PROBLEM SETUP

We now describe the problem setup, whose relevance is illustrated later on through the example of LTV system identification.

#### A. Problem formulation

Our objective is to estimate an unknown and time-varying subspace  $\mathbf{U}_t \in \text{Gr}(n, d)$  online based on possibly noisy data, collected in real-time. We assume that samples  $u_t \in \mathbb{R}^n$  corrupted by additive measurement error  $e_t$  are available from  $\mathbf{U}_t$  at each time, as described in the assumption below.

*Assumption 1:* Each sample  $u_t \in \mathbb{R}^n$  can be decomposed as

$$u_t = \bar{u}_t + e_t,$$

with  $\bar{u}_t \in \mathbf{U}_t$  and  $\|e_t\|_2 \leq \epsilon$  for all  $t \in \mathbb{N}$ .

In addition, we assume an upper bound on the subspace's temporal variability.

*Assumption 2:* There exists some constant  $c \geq 0$  such that  $d_2(\mathbf{U}_t, \mathbf{U}_{t+1}) \leq c$  holds for all  $t \in \mathbb{N}$ .

In case  $c = 0$ , the subspace is independent of time.

Our estimate of the subspace at time  $t$  is denoted by  $\hat{\mathbf{U}}_t \in \text{Gr}(n, d)$ . The uncertainty of this estimate is quantified by an upper bound on its distance to the true subspace  $\mathbf{U}_t$ . Therefore, uncertainty sets are in the form of metric balls of radius  $r$  centered around some subspace  $\mathbf{U} \in \text{Gr}(n, d)$ , defined as

$$\mathbb{B}_r(\mathbf{U}) := \left\{ \hat{\mathbf{U}} \in \text{Gr}(n, d) \mid d_2(\mathbf{U}, \hat{\mathbf{U}}) \leq r \right\}.$$

The problem of interest can now be formulated as follows.

*Problem 1:* Given initial estimate  $\hat{\mathbf{U}}_{t_0}$  at time  $t_0 \in \mathbb{N}$  with  $\hat{\mathbf{U}}_{t_0} \in \mathbb{B}_{r_0}(\mathbf{U}_{t_0})$  for some  $r_0$  and data  $u_t$ ,  $t \in \mathbb{N}$ , find an iterative algorithm that

- provides **uncertainty quantification** in terms of an invariant tube, that is  $\mathbf{U}_t \in \mathbb{B}_{r_t}(\hat{\mathbf{U}}_t)$  for all  $t > t_0$ ,
- is **consistent**, that is,  $\lim_{t \rightarrow \infty} r_t = 0$  as  $c, \epsilon \rightarrow 0$ , and
- is **recursive**, that is,  $\hat{\mathbf{U}}_{t+1}$  depends only on  $\hat{\mathbf{U}}_t$  and the past length- $T$  data window  $u_{\tau}$ ,  $\tau \in \{t - T + 1, \dots, t - 1, t\}$  for some  $1 \leq T \leq t_0 + 1$ .

#### B. Motivating application: online system identification

We illustrate the relevance of our problem setup through the example of identifying LTV systems in the framework of behavioral systems theory [9]. Consider first a state-space representation of a time-varying linear system describing the relationship between inputs and outputs as

$$\begin{aligned} x_{t+1} &= A_t x_t + B_t v_t, \\ y_t &= C_t x_t + D_t v_t, \end{aligned} \quad (2)$$

with state  $x_t \in \mathbb{R}^k$  and time-dependent matrices  $A_t \in \mathbb{R}^{k \times k}$ ,  $B_t \in \mathbb{R}^{k \times m}$ ,  $C_t \in \mathbb{R}^{p \times k}$  and  $D_t \in \mathbb{R}^{p \times m}$ . The input and output trajectories on the time interval  $[t, t+L]$  are defined as  $v_{[t, t+L]} = [v_t^{\top}, \dots, v_{t+L}^{\top}]^{\top}$  and  $y_{[t, t+L]} = [y_t^{\top}, \dots, y_{t+L}^{\top}]^{\top}$ , and they can be expressed using (2) in the form

$$\begin{bmatrix} v_{[t, t+L]} \\ y_{[t, t+L]} \end{bmatrix} = \underbrace{\begin{bmatrix} 0 & I_{m(L+1)} \\ \mathcal{O}_{[t, t+L]} & \mathcal{T}_{[t, t+L]} \end{bmatrix}}_{=: \Lambda_t} \begin{bmatrix} x_t \\ v_{[t, t+L]} \end{bmatrix}, \quad (3)$$

where the matrices  $\mathcal{O}_{[t,t+L]} \in \mathbb{R}^{p(L+1) \times k}$  and  $\mathcal{T}_{[t,t+L]} \in \mathbb{R}^{p(L+1) \times m(L+1)}$  are defined as

$$\mathcal{O}_{[t,t+L]} = \begin{bmatrix} C_t \\ C_{t+1}A_t \\ C_{t+2}A_{t+1}A_t \\ \vdots \\ C_{t+L}A_{t+L-1} \cdots A_t \end{bmatrix},$$

$$\mathcal{T}_{[t,t+L]} = \begin{bmatrix} D_t & 0 & 0 & \cdots & 0 \\ C_{t+1}B_t & D_{t+1} & 0 & \cdots & 0 \\ C_{t+2}A_{t+1}B_t & C_{t+2}B_{t+1} & D_{t+2} & \cdots & 0 \\ \vdots & \vdots & \vdots & \ddots & \vdots \\ C_{t+L}A_{t+L-1} \cdots A_{t+1}B_t & \cdots & \cdots & \cdots & D_{t+L} \end{bmatrix}.$$

The matrix  $\mathcal{O}_{[t,t+L]}$  is related to the observability of the system [38]. If it has full column rank, the matrix  $\Lambda_t$  has full rank, i.e., it spans a subspace of dimension  $k + m(L+1)$ .

Instead of identifying the matrices  $A_t, B_t, C_t$  and  $D_t$ , we focus on identifying the set of all input-output trajectories on the interval  $[t, t+L]$ , which is called the *restricted behavior* [10]. The theoretical foundations of this system description is the subject of behavioral systems theory [9]. The restricted behavior for the LTV system represented by (2) is defined as

$$\mathcal{B}_{[t,t+L]} = \left\{ \begin{bmatrix} v_{[t,t+L]} \\ y_{[t,t+L]} \end{bmatrix} \in \mathbb{R}^{(p+m)(L+1)} \mid \right.$$

$$\left. \exists x_t \text{ such that } x_{[t,t+L]}, v_{[t,t+L]}, y_{[t,t+L]} \text{ satisfy (2)} \right\}.$$

Due to the linearity of equation (3), the restricted behavior  $\mathcal{B}_{[t,t+L]}$  is a subspace spanned by the columns of  $\Lambda_t$ . As the system is time-varying, the restricted behavior changes over time in general.

In light of the above, online identification of LTV systems in the behavioral setting is equivalent to tracking the time-varying subspace  $\mathcal{B}_{[t,t+L]}$ , and thus, it can be formulated as Problem 1. At each time  $t$ , a sample  $[v_{[t-L,t]}^\top, y_{[t-L,t]}^\top]^\top$  from the subspace  $\mathcal{B}_{[t-L,t]}$  can be constructed from the most recent input-output measurements. The proposed problem formulation allows us to handle additive measurement error on the inputs and outputs, c.f., Assumption 1. Furthermore, the upper bound on the distance between two consecutive subspaces in Assumption 2 naturally quantifies how fast the behavior changes. Note that if the matrices  $A_t, B_t, C_t$  and  $D_t$  vary slowly with time, the change in the matrix on the right-hand side of equation (3) is small, and hence,  $d_2(\mathcal{B}_{[t,t+L]}, \mathcal{B}_{[t+1,t+L+1]})$  can be bounded (c.f., [39]). Furthermore, the uncertainty characterization of the identified behavior is useful for various downstream tasks, such as prediction, estimation, or control. For example, it can be used to quantify the uncertainty of predicted trajectories, or to robustify control formulations. Besides describing time-varying systems, LTV models are also often used to approximate the behavior of nonlinear systems [15], [16].

Even though the state-space representation (2) can be related to the restricted behavior through the equation (3), we do not aim at recovering the matrices  $A_t, B_t, C_t$  and  $D_t$  to form an estimate of  $\mathcal{B}_{[t,t+L]}$ . Instead, we use the subspace estimate and its uncertainty quantification directly to perform downstream tasks, such as prediction, which is described

below and illustrated in Section V-B. We divide the input-output trajectories into initial and future parts of length  $T_{\text{ini}}$  and  $T_{\text{fut}}$ , respectively, i.e.,  $v_{[t-T_{\text{ini}}+1,t+T_{\text{fut}}]} = [v_{\text{ini}}^\top, v_{\text{fut}}^\top]^\top$  and  $y_{[t-T_{\text{ini}}+1,t+T_{\text{fut}}]} = [y_{\text{ini}}^\top, y_{\text{fut}}^\top]^\top$ . Let  $\hat{U}$  be a basis for the estimated behavior  $\mathcal{B}_{[t-T_{\text{ini}}+1,t+T_{\text{fut}}]}$ . We denote the block-rows of  $\hat{U}$  corresponding to each trajectory component by  $\hat{U}^{v_{\text{ini}}}, \hat{U}^{y_{\text{ini}}}, \hat{U}^{v_{\text{fut}}}$ , and  $\hat{U}^{y_{\text{fut}}}$ . Given  $v_{\text{ini}}, y_{\text{ini}}, v_{\text{fut}}$ , the future outputs at times  $t+1, \dots, t+T_{\text{fut}}$  are predicted as  $\hat{y}_{\text{fut}} = M[v_{\text{ini}}^\top, y_{\text{ini}}^\top, v_{\text{fut}}^\top]^\top$ , with  $M$  defined as

$$M := \hat{U}^{y_{\text{fut}}} \begin{bmatrix} \hat{U}^{v_{\text{ini}}} \\ \hat{U}^{y_{\text{ini}}} \\ \hat{U}^{v_{\text{fut}}} \end{bmatrix}^\dagger,$$

where  $\dagger$  denotes the Moore-Penrose pseudoinverse. This linear multi-step predictor originates from the classic and widely adopted Subspace Predictive Control [13], [40].

#### IV. SUBSPACE TRACKING WITH GUARANTEES

Our main results are presented in this section. In Section IV-A, we discuss how the signal in the data can be distinguished from noise. Then, we introduce the gradient descent method in Section IV-B that serves as the main building block of the subspace tracking algorithm proposed in Section IV-C.

##### A. Distinguishing between signal and noise

In this section, we define and analyze the signal and noise components of the online data. We consider a data window of length  $T \geq d$  consisting of the most recent samples up to time  $t$  organized into a matrix

$$W_t = [u_{t-T+1} \ u_{t-T+2} \ \cdots \ u_t] \in \mathbb{R}^{n \times T}, \quad t \in \mathbb{Z}_{\geq T}.$$

Our goal is to estimate the current subspace  $\mathbf{U}_t$  using the data matrix  $W_t$ . However, as the system is time-varying, only the last sample  $u_t$  originates from  $\mathbf{U}_t$ . Therefore, instead of using the nominal sample  $\bar{u}_t$  and the measurement error  $e_t$  from Assumption 1, we characterize the signal and noise components of  $W_t$  by introducing the following decomposition:

$$W_t = P_{\mathbf{U}_t} W_t + P_{\mathbf{U}_t}^\perp W_t.$$

The first term lies in  $\mathbf{U}_t$  and is defined to be the signal, while the second term lies in the orthogonal complement of  $\mathbf{U}_t$  and is considered as noise (see Figure 1 for an illustration). Under the stated assumptions, the noise term can be bounded as follows. The proof can be found in the Appendix.

*Lemma 2 (Noise bound):* Let Assumptions 1 and 2 hold. Then,

$$\|P_{\mathbf{U}_t}^\perp W_t\|_F \leq \delta_t, \quad \forall t \geq T \quad (4)$$

where  $\delta_t \geq 0$  is strictly monotone in  $\epsilon$  and  $c$ , defined as

$$\delta_t := c \|W_t D\|_F + \epsilon \sqrt{T} (c(T-1) + 1),$$

with  $D := \text{diag}(T-1, T-2, \dots, 0)$ .

Lemma 2 guarantees that the noise component  $P_{\mathbf{U}_t}^\perp W_t$ , which captures both the (slowly) time-varying nature of the subspace and the effect of measurement error, is bounded by the

function  $\delta_t$ . To be able to guarantee positive convergence rate for the updates in the subsequent section, we also impose bounds on the singular values of the signal component  $P_{\mathbf{U}_t} W_t$ .

*Assumption 3:* There exists constants  $0 < \underline{\sigma} \leq \bar{\sigma}$  such that the matrix  $W_t$  satisfies  $\sigma_1(P_{\mathbf{U}_t} W_t) \leq \bar{\sigma}$  and  $\sigma_d(P_{\mathbf{U}_t} W_t) \geq \underline{\sigma}$  for all  $t \in \mathbb{Z}_{\geq T}$ .

The upper bound can be trivially satisfied by choosing  $\bar{\sigma} = \sigma_1(W_t) = \|W_t\|_2$ . Furthermore, the lower bound ensures that the signal term  $P_{\mathbf{U}_t} W_t$  spans  $\mathbf{U}_t$  as illustrated in Figure 1.

*Remark 1:* Lemma 2 and Assumption 3 are related to system identification described in Section III-B as follows. Each sample  $u_t$  is an  $L + 1$  step long input-output trajectory  $[v_{[t-L,t]}^\top, y_{[t-L,t]}^\top]^\top$ , and therefore,  $W_t$  is the  $L + 1$  deep Hankel matrix associated with  $v$  and  $y$ . Suppose that the data is generated by an observable LTI system, implying  $\mathbf{U}_t = \mathbf{U}_{t+1} = \mathbf{U}$  for all  $t \in \mathbb{Z}_{\geq T}$ , and therefore,  $c = 0$ . Assume further that the input-output data are measured exactly, i.e.,  $\epsilon = 0$ . Under these assumptions, the bound in Lemma 2 reduces to  $\delta_t \equiv 0$ . Consequently, it holds that  $W_t \in \mathbf{U}$ , i.e., all measured trajectories of length  $L + 1$  must lie in a subspace of dimension  $k + m(L + 1)$ , which is in line with the linearity and time-invariance of the system. Furthermore, the condition  $\sigma_d(P_{\mathbf{U}_t} W_t) \geq \underline{\sigma} > 0$  from Assumption 3 ensures that the singular values of the Hankel matrix  $W_t$  are lower bounded by  $\underline{\sigma}$ . This can be guaranteed by imposing a *quantitative persistency of excitation* condition on the input sequence, which is formalized in [41], [42]. ■

*Remark 2:* Both the noise bound  $\delta_t$  in Lemma 2 and the lower bound  $\underline{\sigma}$  on the signal in Assumption 3 grow as the window length  $T$  increases. On the one hand, samples from "older" subspaces are included in the data matrix  $W_t$  for larger  $T$ , possibly leading to larger noise contribution. On the other hand, including more data also increases the signal in  $W_t$ . In fact, the lower bound  $\sigma_d(P_{\mathbf{U}_t} W_t) \geq \underline{\sigma} > 0$  in Assumption 3 can only be satisfied if  $T \geq d$  holds. From a practical perspective, the choice of  $T$  provides a tuning parameter to control the rate of adaptation of the tracking algorithm introduced in Section IV-C. A shorter data window leads to faster adaptation, yet choosing  $T$  too small increases the sensitivity to disturbances. One can tune the value of  $T$ , e.g., by validation, which is demonstrated in the numerical example in Section V-B. ■

## B. Gradient descent on the Grassmannian

The main idea of our approach is to update a subspace estimate each time a new sample is available by performing  $K$  iterations of gradient descent on the Grassmannian manifold. Due to the simplicity of the gradient descent update rule, we are able to provide strong theoretical guarantees for the resulting algorithm. We denote the estimate at iteration  $k$  by  $\Gamma_k$ . Since estimates are points on the Grassmannian manifold, the optimization is carried out intrinsically on the manifold as described below.

As discussed in the previous section, the data matrix  $W_t$  serves as a surrogate representation to the true (unknown) subspace  $\mathbf{U}_t$ . Therefore, we use the projection error of  $W_t$

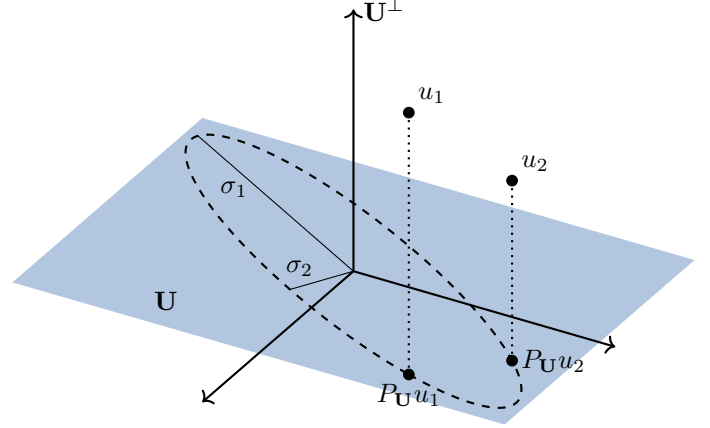


Fig. 1. Illustration of the signal-to-noise ratio properties on a two dimensional subspace  $\mathbf{U}$  in  $\mathbb{R}^3$  (shaded). Two data samples,  $u_1$  and  $u_2$  are depicted along with their noise components (dotted lines). The signal component  $P_{\mathbf{U}} W$  with  $W = [u_1 \ u_2]$  is illustrated by the dashed ellipse, with  $\sigma_1$  and  $\sigma_2$  being the two singular values. Note that the ellipse lies in the plane  $\mathbf{U}$ , and we omitted the subscript  $t$  throughout.

onto  $\Gamma_k$  as the cost for the gradient descent:

$$F_{W_t}(\Gamma_k) := \sum_{i=0}^{T-1} \|P_{\Gamma_k}^\perp u_{t-i}\|_2^2 = \|P_{\Gamma_k}^\perp W_t\|_F^2. \quad (5)$$

It is worth noting that if  $W_t = U_t$ , the cost function reduces to the squared chordal distance, i.e.,  $F_{U_t}(\Gamma_k) = d_2(\Gamma_k, \mathbf{U}_t)^2$  holds. Using (1), the Riemannian gradient of the cost is

$$\begin{aligned} \text{grad } F_{W_t}(\Gamma_k) &= P_{\Gamma_k}^\perp \nabla F_{W_t}(\Gamma_k) \\ &= P_{\Gamma_k}^\perp \nabla \text{tr}(W_t^\top P_{\Gamma_k}^\perp W_t) \\ &= -2P_{\Gamma_k}^\perp W_t W_t^\top \Gamma_k. \end{aligned} \quad (6)$$

We use the exponential map to take a step of size  $\alpha > 0$  towards the negative gradient direction, yielding the update

$$\begin{aligned} \Gamma_{k+1} &= \text{Exp}_{\Gamma_k}(-\alpha \text{grad } F_{W_t}(\Gamma_k)) \\ &= [\Gamma_k Q_2 \ Q_1] \begin{bmatrix} \cos(-\alpha S) \\ \sin(-\alpha S) \end{bmatrix} Q_2^\top, \end{aligned} \quad (7)$$

where  $\text{grad } F_{W_t}(\Gamma_k) = Q_1 S Q_2$  is the compact SVD. We use a constant step size for the update to streamline the analysis. However, the performance of the algorithm can be improved by optimizing the step size online (e.g., via line search), as illustrated in the numerical example in Section V-B.

*Remark 3:* Another subspace tracking algorithm, termed GROUSE [23], also relies on gradient descent techniques on the Grassmannian manifold. In contrast to our formulation, the GROUSE method minimizes the projection error of the most recent sample only, which is a special case of the proposed method with  $T = 1$  in the cost (5). As a result, the gradient descent step boils down to a rank-one update of the subspace estimate yielding lower computational complexity than that of our algorithm. In [27], the authors analyze the GROUSE algorithm under the crucial assumption that the nominal samples  $\bar{u}_t$  are i.i.d. random variables with support on  $\mathbf{U}_t$ . This condition allows them to prove convergence of the estimates in expectation. However, the assumption does not hold if the

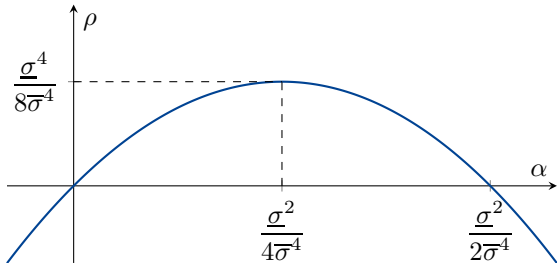


Fig. 2. Illustration of the convergence rate  $\rho$  as a function of the step size  $\alpha$  in Lemma 3. The convergence rate is positive for any  $\alpha$  from the interval  $(0, \frac{\sigma^2}{2\sigma^4})$ . The maximal value of  $\rho$  is  $\frac{\sigma^4}{8\sigma^4}$ , which is achieved with  $\alpha = \frac{\sigma^2}{4\sigma^4}$ .

subspace represents a dynamical system (c.f., Sec. III-B), where samples are correlated. In our setup, on the other hand, a moving data window consisting of  $T \geq d$  samples is used in the cost. This enables us to impose Assumption 3, which can be satisfied by subspaces representing dynamical systems. Under this assumption, we can guarantee monotonic improvement of the subspace estimates in Lemma 3. ■

The following enabling lemma establishes guarantees on the evolution of the distance between the estimate and the true subspace under the update rule (7).

*Lemma 3 (Single step decay bound):* Suppose Assumptions 1, 2 and 3 hold and let  $r > 0$ . Then, for all  $\mathbf{\Gamma}_k \in \mathbb{B}_r(\mathbf{U}_t)$  and all  $k \in [0, K-1]$ ,  $t \in \mathbb{Z}_{\geq T}$

$$d_2(\mathbf{\Gamma}_{k+1}, \mathbf{U}_t)^2 \leq d_2(\mathbf{\Gamma}_k, \mathbf{U}_t)^2 - \rho \|\text{grad } d_2(\mathbf{\Gamma}_k, \mathbf{U}_t)\|_F^2 + \gamma_r(\delta_t),$$

where  $\rho := \alpha\bar{\sigma}^2 - 2\alpha^2\bar{\sigma}^4$  and  $\gamma_r \in \mathcal{K}_\infty$  is

$$\begin{aligned} \gamma_r(\delta_t) := & 8\alpha r \bar{\sigma} (1 + 4\alpha \bar{\sigma}^2) \delta_t + (4\alpha r + 16\alpha^2 \bar{\sigma}^2 (r + 2)) \delta_t^2 \\ & + 32\alpha^2 \bar{\sigma} \delta_t^3 + 8\alpha^2 \delta_t^4, \end{aligned}$$

with  $\delta_t \geq 0$  defined in (4).

Lemma 3 provides a bound on the improvement of the estimate during a single gradient descent step. The improvement in the chordal distance between the estimate and the true subspace is proportional to the squared gradient norm times the constant  $\rho$ , which is related to the signal part of  $W_t$ . On the other hand, the noise part of  $W_t$  deteriorates the guaranteed improvement. This effect is characterized by the bias term  $\gamma_r(\delta_t)$ , where  $\gamma_r$  is a fourth-order polynomial in the noise bound  $\delta_t$  from Lemma 2. Since all coefficients are non-negative, and the constant coefficient is zero,  $\gamma_r$  is a  $\mathcal{K}_\infty$  function. Therefore, for the noise-free case with  $\delta_t \equiv 0$  (c.f., Remark 1), Lemma 3 guarantees monotonic improvement of the estimates as long as the gradient of  $d_2(\mathbf{\Gamma}_k, \mathbf{U}_t)$  is non-zero, and the step size is sufficiently small. More specifically, if the step size  $\alpha$  is in the interval  $(0, \frac{\sigma^2}{2\sigma^4})$ ,  $\rho$  is guaranteed to be positive; see Figure 2 and the later Remark 6 for a more detailed discussion. Note that the bound in Lemma 3 is tighter for smaller radius  $r$ , i.e., when the estimate  $\mathbf{\Gamma}_k$  is closer to  $\mathbf{U}_t$ .

### C. Tracking of time-varying subspaces

The proposed method for tracking  $\mathbf{U}_t$  called *Grassmannian Recursive Algorithm for Tracking* (GREAT) is summarized by the pseudo-code in Algorithm 1.

---

#### Algorithm 1 GREAT

---

**Input:** initial estimate  $\hat{\mathbf{U}}_{t_0} \in \text{Gr}(n, d)$ , sequence of samples  $\{u_t\}_{t \geq 1}$ , window length  $T \in [1, t_0 + 1]$ , step size  $\alpha \in (0, \frac{\sigma^2}{2\sigma^4})$ , gradient descent iteration number  $K > 0$

**for**  $t = t_0 + 1, t_0 + 2, \dots$

    Construct matrix  $W_t = [u_{t-T+1} \ u_{t-T+2} \ \dots \ u_t]$

    Initialize gradient descent  $\mathbf{\Gamma}_0 = \hat{\mathbf{U}}_{t-1}$

**for**  $k = 0, \dots, K-1$

        Grad. descent step  $\mathbf{\Gamma}_{k+1} = \text{Exp}_{\mathbf{\Gamma}_k}(-\alpha \text{grad } F_{W_t}(\mathbf{\Gamma}_k))$

**end**

    Update estimate  $\hat{\mathbf{U}}_t = \mathbf{\Gamma}_K$

**end**

**Output:** sequence of estimates  $\{\hat{\mathbf{U}}_t\}_{t > t_0}$

---

The GREAT algorithm recursively updates the subspace estimate  $\hat{\mathbf{U}}_t$  by performing  $K$  steps of gradient descent update (7) between sampling times  $t$  and  $t+1$ . The initial estimate  $\hat{\mathbf{U}}_{t_0}$  can be constructed as the span of  $d$  singular vectors of an initializing data matrix  $W_{\text{ini}} = [u_1 \ u_2 \ \dots \ u_{t_0}]$ , corresponding to its largest singular values. With this choice,  $\hat{\mathbf{U}}_{t_0}$  becomes the minimizer of the cost  $F(\hat{\mathbf{U}}) = \|P_{\hat{\mathbf{U}}}^\perp W_{\text{ini}}\|_F^2$  (c.f., Eq. (5)). During online operation, the data matrix  $W_t$  is constructed from the most recent samples, and therefore, the subspace estimates adapt to the online data.

*Remark 4:* The computationally most expensive part of Algorithm 1 is calculating the gradient of the cost in equation (6) at each gradient descent iteration. For an efficient implementation, one can exploit that the data matrix only appears as an inner product  $W_t W_t^\top$  (the empirical data covariance) in the expression. This inner product at time  $t$  can be formulated as a rank-2 update, i.e.,  $W_t W_t^\top = W_{t-1} W_{t-1}^\top - u_{t-T} u_{t-T}^\top + u_t u_t^\top$ . Therefore, the complexity of the algorithm does not depend on  $T$ . With this implementation, the asymptotic complexity of computing the gradient is  $\mathcal{O}(n^2 d)$ , leading to overall complexity  $\mathcal{O}(K n^2 d)$  per sample. The other expensive part of the algorithm is evaluating the exponential map in equation (7), which requires computing the compact SVD of the gradient. However, that step is of complexity  $\mathcal{O}(n d^2)$  only, and therefore it is not the bottleneck. Similarly to Algorithm 1, various data-driven control formulations depend only on the empirical data covariance, and this fact was exploited for computational reasons, e.g., in [43]. ■

Now we turn to the theoretical analysis of Algorithm 1. We provide convergence guarantees for the GREAT algorithm by utilizing the bound in Lemma 3 that quantifies the improvement of the inner loop with the gradient descent update. In addition, we exploit the fact that the chordal distance is gradient dominant if  $d_2(\mathbf{\Gamma}_k, \mathbf{U}_t) \leq r_b$  holds for some  $r_b < 1$ . To show that this condition always holds, we first require that the initial estimate falls in the ball  $\mathbb{B}_{r_b}$  centered around the true subspace. Further, we assume that the ratio between the signal and noise in  $W_t$  is such that the gradient descent steps in the inner loop keep the estimates close to the changing true subspace (see Figure 3). These conditions are formalized in the following assumption.

*Assumption 4:* Suppose that the initial estimate satisfies

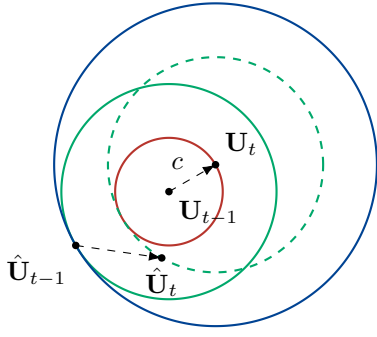


Fig. 3. Illustration of Assumption 4 and Lemma 4. If the estimate  $\hat{\mathbf{U}}_{t-1}$  is in the metric ball  $\mathbb{B}_{r_b-c}(\mathbf{U}_{t-1})$  (solid green circle), it is also in  $\mathbb{B}_{r_b}(\mathbf{U}_t)$  (blue circle), since  $\mathbf{U}_t \in \mathbb{B}_c(\mathbf{U}_{t-1})$  (red circle) holds by Assumption 2. Furthermore, under Assumption 4, the gradient descent updates in the inner loop of the GREAT algorithm guarantee that the distance between the estimate and  $\mathbf{U}_t$  reduces from  $r_b$  to  $r_b - c$ , i.e.,  $\hat{\mathbf{U}}_t \in \mathbb{B}_{r_b-c}(\mathbf{U}_t)$  (dashed green circle). Therefore, the estimates are always contained in the ball  $\mathbb{B}_{r_b}$  centered around the current true subspace.

$\hat{\mathbf{U}}_{t_0} \in \mathbb{B}_{r_b}(\mathbf{U}_{t_0+1})$  for some  $c \leq r_b < 1$ . Furthermore, we assume that for all  $t \in \mathbb{Z}_{\geq t_0}$

$$\gamma_{r_b}(\delta_t) \leq (1 - \tilde{\rho})r_b^2 + \frac{(1 - \tilde{\rho})(c^2 - 2cr_b)}{1 - \tilde{\rho}^K}, \quad (8)$$

with  $\tilde{\rho} := 1 - 4(1 - r_b^2)(\alpha\bar{\sigma}^2 - 2\alpha^2\bar{\sigma}^4) \geq 0$ .

The assumption provides a condition that depends both on the design parameters  $\alpha, T, K$ , and the constants  $\epsilon, c, \underline{\sigma}, \bar{\sigma}$  from Assumptions 1-3 quantifying the properties of the data. For fixed design parameters, inequality (8) can be interpreted as a lower bound on the signal-to-noise ratio of the data matrix  $W_t$ . The right-hand side grows with  $\underline{\sigma}$ , which characterizes the signal part of  $W_t$ . By contrast, the left-hand side is related to the noise bound  $\delta_t$  through the  $\mathcal{K}_\infty$  function  $\gamma_{r_b}$ .

*Remark 5:* In case only one gradient descent iteration is performed in the inner loop of Algorithm 1, i.e.,  $K = 1$  holds, the condition (8) can be expressed as

$$\underline{\sigma}^2 \geq \frac{\gamma_{r_b}(\delta_t) + c(2r_b - c)}{4\alpha r_b^2(1 - r_b^2)} + 2\alpha\bar{\sigma}^4.$$

This condition is an explicit lower bound on the signal component of  $W_t$ . Note that the bound increases if  $c$  grows, as  $c \leq r_b$  must hold. ■

With these assumptions in place, we conclude that the estimates always lie in the ball  $\mathbb{B}_{r_b}$  around the true sequence of subspaces, see Figure 3 for an illustration. In this set, the chordal distance satisfies a gradient dominance property, as formalized below:

*Lemma 4 (Gradient dominance):* Let Assumptions 1, 2, 3 and 4 hold. Then, the estimates in Algorithm 1 satisfy for all  $t \in \mathbb{Z}_{\geq t_0}$  and all  $k = 0, \dots, K$

- 1)  $\mathbf{\Gamma}_k \in \mathbb{B}_{r_b}(\mathbf{U}_t)$ ,
- 2)  $\|\text{grad } d_2(\mathbf{\Gamma}_k, \mathbf{U}_t)\|_F^2 \geq 4(1 - r_b^2)d_2(\mathbf{\Gamma}_k, \mathbf{U}_t)^2$ .

We are now ready to analyze how the distance between the true subspace and the estimate evolves under Algorithm 1.

*Theorem 1 (Convergence and uncertainty quantification):* Let Assumptions 1, 2, 3 and 4 hold. Then, the output

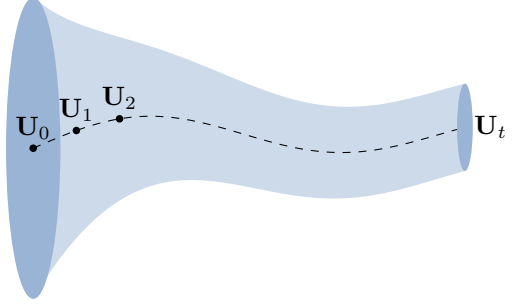


Fig. 4. Illustration of the bound in Theorem 1. The blue tube illustrates a sequence of metric balls with varying radius centered around the true sequence of subspaces (dashed line). The estimates from the GREAT algorithm are guaranteed to remain in the tube. The evolution of the tube's radius is a function of the bound on the true subspace's rate of change  $c$ , the measurement error  $\epsilon$ , and the signal  $\bar{\sigma}, \underline{\sigma}$ .

$\{\hat{\mathbf{U}}_t\}_{t > t_0}$  of Algorithm 1 is such that

$$\begin{aligned} d_2(\hat{\mathbf{U}}_t, \mathbf{U}_t)^2 &\leq \tilde{\rho}^{Kt} d_2(\hat{\mathbf{U}}_{t_0}, \mathbf{U}_{t_0})^2 + \frac{1 - \tilde{\rho}^{Kt}}{1 - \tilde{\rho}} \gamma_{r_b}(\|\delta\|_\infty) \\ &\quad + \frac{1 - \tilde{\rho}^{Kt}}{1 - \tilde{\rho}^K} \tilde{\rho}^K (2r_b - c)c, \quad \forall t \in \mathbb{Z}_{\geq t_0+1}, \end{aligned} \quad (9)$$

where  $\tilde{\rho} \in (0, 1)$  for  $\alpha$  satisfying  $0 < \alpha < \frac{\sigma^2}{2\bar{\sigma}^4}$ . Consequently, the following ultimate bound is satisfied

$$\begin{aligned} \limsup_{t \rightarrow \infty} d_2(\hat{\mathbf{U}}_t, \mathbf{U}_t)^2 &= \frac{1}{1 - \tilde{\rho}} \gamma_{r_b}(\|\delta\|_\infty) \\ &\quad + \frac{\tilde{\rho}^K}{1 - \tilde{\rho}^K} (2r_b - c)c. \end{aligned} \quad (10)$$

The proof of Theorem 1 can be found in the Appendix, and follows by combining the single step improvement bound in Lemma 3 and the gradient dominance property in Lemma 4. Theorem 1 guarantees that the subspace estimate remains in an invariant tube around the true sequence of subspaces as illustrated in Figure 4. The tube is characterized by the squared chordal distance between  $\hat{\mathbf{U}}_t$  and  $\mathbf{U}_t$ . Inequality (9) quantifies how the tube size (also called bias) is affected by the measurement error  $\epsilon$  on the data and time variation  $c$  of the true subspace affecting the noise portion of the measurements in (4). Less noise in the samples and/or slower variation of the true subspace leads to a smaller uncertainty region. Furthermore, the ultimate bound in (10) captures the asymptotic behavior of the tube size.

Note that the GREAT algorithm produces consistent estimates in the sense that  $\lim_{t \rightarrow \infty} d_2(\hat{\mathbf{U}}_t, \mathbf{U}_t) = 0$  for  $c = \epsilon = 0$ . Furthermore, exponential convergence to the true subspace can be guaranteed in this case, which is summarized in the following corollary:

*Corollary 1 (Consistency):* Let Assumptions 1, 2, 3 and 4 hold, and suppose that  $\epsilon, c = 0$ . Then, the output  $\{\hat{\mathbf{U}}_t\}_{t > t_0}$  of Algorithm 1 is such that

$$d_2(\hat{\mathbf{U}}_t, \mathbf{U}_t)^2 \leq \tilde{\rho}^{Kt} d_2(\hat{\mathbf{U}}_{t_0}, \mathbf{U}_{t_0})^2, \quad \forall t \in \mathbb{Z}_{\geq t_0+1}.$$

The claim directly follows from equation (9), the definition of  $\delta_t$  in (4), and the fact that  $\gamma_{r_b} \in \mathcal{K}_\infty$ . The condition  $c = \epsilon = 0$  holds true, e.g., when LTI systems are identified from exact measurements (c.f., Rem. 1).

*Remark 6:* The step size of the gradient descent update in Algorithm 1 is an important tuning parameter. Choosing its value from the interval  $(0, \underline{\sigma}^2/(2\bar{\sigma}^4))$  guarantees that  $\rho \in (0, 1/8)$ ; see Figure 2 for a visualization. Further, this guarantees that the bound in inequality (9) converges, as  $\tilde{\rho} = 1 - 4(1 - r_b^2)\rho \in (0, 1)$  holds. The maximal convergence rate (minimal  $\tilde{\rho}$ ) is achieved with  $\alpha = \alpha^{\text{cvg}} = \underline{\sigma}^2/(4\bar{\sigma}^4)$ . On the other hand, the ultimate bound in equation (10) is also affected by the step size. Namely,  $\tilde{\rho}$  and  $\gamma_r$  defined in Lemma 3 and Assumption 4 are rational functions of  $\alpha$ . One can find the step size  $\alpha^{\text{ub}}$  numerically, for which the ultimate bound is minimized. The trade-off between these conflicting objectives is illustrated in the numerical example in Section V-A. ■

*Remark 7:* Inequality (9) can be interpreted through the lens of nonlinear control, revealing a parallel to input-to-state inequalities [44]. Specifically, the noise bound  $\delta_t$  and the time-variation bound  $c$  on the true subspace may be regarded as exogenous inputs. When the input is zero, the inequality ensures that the system's state decays in some norm, analogous to the squared distance  $d_2(\hat{\mathbf{U}}_t, \mathbf{U}_t)^2$  in our setup (see Corollary 1). For non-zero inputs,  $d_2(\hat{\mathbf{U}}_t, \mathbf{U}_t)^2$  remains bounded, with the bound scaling with the input size, as illustrated in (10). ■

*Remark 8:* We note that it is also possible to achieve adaptation by discounting the past data via an exponential forgetting factor  $0 < \gamma < 1$ . In this case, we can utilize all past data by defining the data matrix  $W_t$  as

$$W_t = [\gamma^{t-1}u_1 \ \gamma^{t-2}u_2 \ \dots \ \gamma^0u_t].$$

Even though the number of columns in  $W_t$  grows over time, the final computations are not affected, since the matrix  $W_t$  only appears as an inner product  $W_t W_t^\top$ , see Remark 4. This can be computed by a rank-1 update as  $W_{t+1} W_{t+1}^\top = \gamma^2 W_t W_t^\top + u_{t+1} u_{t+1}^\top$ . Alternatively, one can also combine the two approaches by considering a moving data window with discounted past data. The theoretical analysis incorporating forgetting factors leads to a different bound in Lemma 2, which can be derived following similar arguments. ■

## V. NUMERICAL CASE STUDIES

This section presents two numerical case studies. First, we illustrate the theoretical properties of the proposed method through a synthetic example. Second, we demonstrate how the GREAT algorithm can be applied to online system identification as described in Section III-B. This example considers an LTV airplane model adopted from the literature. The MATLAB code reproducing both case studies is available online at [https://gitlab.ethz.ch/asasfi/ST\\_for\\_sysID](https://gitlab.ethz.ch/asasfi/ST_for_sysID).

### A. Tracking a random geodesic

The goal of this synthetic example is to assess the conservatism of the bounds in Theorem 1 and to illustrate the trade-off when selecting the step size  $\alpha$ , described in Remark 6.

To better highlight the conservatism originating from the analysis, we construct the example such that the bounds in Assumptions 1-3 are tight. We generate a reference sequence of subspaces  $\mathbf{U}_t \in \text{Gr}(5, 3)$  for  $t = 0, \dots, 150$  defined by a geodesic that starts from an initial subspace  $\mathbf{U}_0$  and follows a tangent direction  $V$ . The initial subspace  $\mathbf{U}_0$  is spanned by the first 3 unit vectors in  $\mathbb{R}^5$ . To generate a direction  $V$ , we first sample a matrix randomly from a standard normal distribution and then project it onto the tangent space of  $\mathbf{U}_0$ . The spacing between consecutive subspaces is chosen such that Assumption 2 holds with  $c = 5 \cdot 10^{-5}$ . The samples are generated as  $u_t = U_t \xi_t + e_t$ , with  $\xi_t \sim \mathcal{N}(0, I_3)$  and  $e_t \sim \mathcal{N}(0, I_5)$ , and  $e_t$  was scaled such that  $\|e_t\|_2 = \epsilon = 10^{-3}$  for all  $t = 1, \dots, 150$  (c.f., Asm. 1). We choose the data window length to be  $T = 100$ , and perform  $K = 10$  iterations of the gradient descent method at each time  $t$ . The constants with values  $\underline{\sigma} = 8.49$  and  $\bar{\sigma} = 11.28$  were computed, such that the inequalities in Assumption 3 are tight on the time interval  $t = [100, 150]$ . The initial estimate  $\hat{\mathbf{U}}_{99}$  is chosen from the set  $\mathbb{B}_{r_b}(\mathbf{U}_{100})$  with  $r_b = 0.1$ . We note that Assumption 4 is satisfied with the provided parameters.

We compute  $\alpha^{\text{ub}}$  (c.f., Remark 6) by minimizing the ultimate bound using the *fmincon* function of Matlab, and run the algorithm on the same dataset with step sizes  $\alpha = \left\{ \alpha^{\text{cvg}}, \frac{\alpha^{\text{cvg}} + \alpha^{\text{ub}}}{2}, \alpha^{\text{ub}} \right\}$  to illustrate the trade-off between the convergence rate and the ultimate bound. The distance between the resulting estimates and the true subspace, as well as the theoretical bounds are depicted in Figure 5. Clearly, the fastest convergence is achieved with  $\alpha^{\text{cvg}}$  for both the theoretical bound and the true distance. On the other hand, the smallest ultimate bound is achieved with  $\alpha^{\text{ub}}$  at the expense of slower convergence. In between these edge cases, the intermediate value  $\alpha = 5.78 \cdot 10^{-4}$  provides a good trade-off, achieving both fast convergence and low ultimate bound.

### B. Online system identification

The second example shows how the proposed method can be used for online identification of LTV systems. We compare our approach with two methods from the system identification toolbox of MATLAB that are often used as benchmarks. Namely, we consider the *N4SID* algorithm that estimates a state-space model offline using subspace identification method [32], and with the *recursiveLS* algorithm, that estimates the parameters of a multivariate ARX model online using recursive least squares technique [33]. The identified models will then be used to predict future outputs, and the prediction error is compared. We assume that no prior system knowledge is available, and therefore, the hyperparameters of each identification method must be tuned by validation.

1) *Data generation:* We use the airplane model described in [45] to generate input-output data. Different LTI state-space representations of this third-order system are given under different flight conditions. We simulate the behavior of the airplane when accelerating from 0.9 to 1.5 Mach number at the altitude of 35000 feet by linearly interpolating the elements of the state-space matrices between the two operating conditions. We add a linear state-feedback  $u_{fb} = [-0.09, -0.8, 0]x$  that



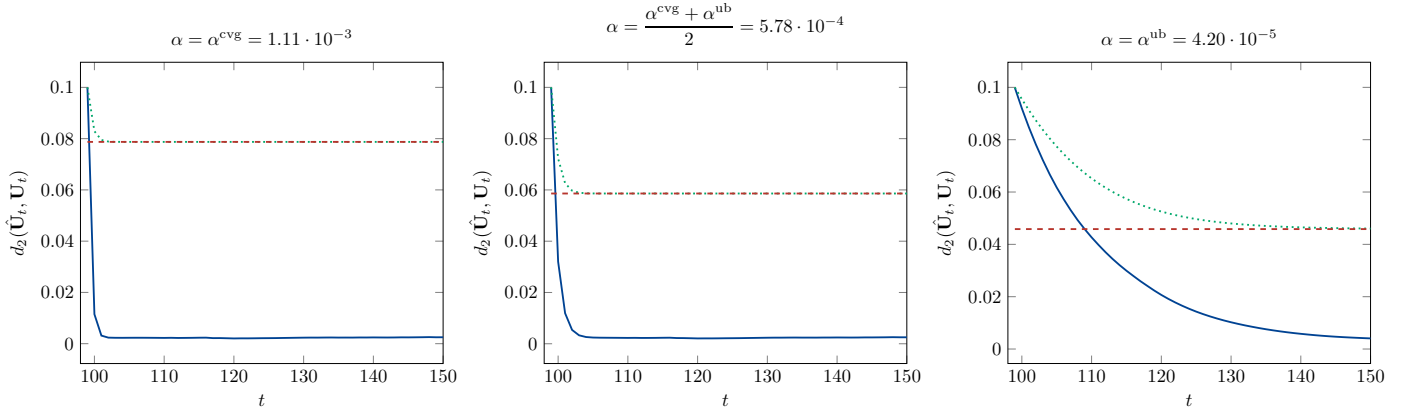


Fig. 5. Illustration of the subspace tracking algorithm GREAT with the derived theoretical bounds. For different step sizes  $\alpha$ , the evolution of the distance between the estimates and the true subspace (blue, solid) is shown with the bound from inequality (9) (green, dotted) and the ultimate bound from equation (10) (red, dashed) in Theorem 1. The step size  $\alpha^{\text{cvg}}$  (left) maximizes the convergence rate, and  $\alpha^{\text{ub}}$  (right) minimizes the ultimate bound (c.f., Remark 6).

is stabilizing in both operating conditions, and discretize the closed-loop system leading to LTV state-space equations in the form (2) with  $C_t \equiv I_3$  and  $D_t \equiv 0$ . We simulate the resulting discrete-time system for 1000 steps starting from zero initial conditions and random inputs drawn from a normal distribution with unit variance. The outputs  $y_t$  are corrupted by additive measurement error, which is also drawn from the normal distribution with variance  $0.01I_3$ . We split the dataset into *training*, *validation*, and *test* parts of equal size. We simulate 100 trajectories in the test part with different input and measurement error realizations to enable statistical analysis of the results.

**2) Implementation details:** We identify the restricted behavior online using the proposed method as described in Section III-B. We select  $L = 9$  for the horizon making the dimension of the embedding space  $n = 40$ . The dimension of the subspace that is related to the system order and the data window length controlling the rate of adaptation (c.f., Remark 2) are chosen as hyperparameters. We select  $d = 13$  and  $T = 120$  from the ranges  $\{11, 12, 13, 14, 15\}$  and  $\{30, 60, 90, 120, 150\}$ , respectively, as they achieve the smallest prediction error on the validation set. The algorithm is initialized as discussed in Section IV-C using the training data. For improved performance, the gradient descent step on the manifold is implemented using the *manopt* toolbox [46], which optimizes the step size online by line-search. The maximal number of steps is limited to  $K = 2$ . We predict the future outputs using the estimated behavior as described in Section III-B with  $T_{\text{ini}} = T_{\text{fut}} = 5$ .

The state-space model is estimated offline by calling the *N4SID* function once on both the training and validation data, and the order of the system is automatically selected<sup>3</sup> as 5 from the interval  $\{1, 2, \dots, 5\}$ . In order to make predictions with the identified model, the state of the system is estimated using a Kalman filter. The noise covariance matrices for the filter are tuned on the validation data. For the ARX

model, the output and input orders (c.f., [33]) are selected as  $n_a = 1$  and  $n_b = 3$ , respectively, both from the interval  $\{1, 2, \dots, 10\}$ . The rate of adaptation is controlled by the forgetting factor, which is judiciously selected as 0.985 from the range  $\{0.98, 0.985, 0.99, 0.995, 1\}$  by validation. The initial coefficients are computed by minimizing the prediction error on the training data.

**3) Results:** We compare the different identification methods by their predictive performance on the test set. The prediction error is computed for all 100 trajectories. The subspace estimate and the ARX model parameters are updated online. We do not update the state-space model as the *N4SID* function of the system identification toolbox does not support adaptation. At time  $t$ , we predict the next  $T_{\text{fut}} = 5$  outputs denoted by  $\hat{y}_i$ ,  $i = t + 1, \dots, t + T_{\text{fut}}$ . The relative error is given as

$$\text{relative prediction error} = \sqrt{\frac{\sum_{i=t+1}^{t+T_{\text{fut}}} \|\hat{y}_i - y_i\|^2}{\sum_{i=t+1}^{t+T_{\text{fut}}} \|y_i\|^2}}.$$

The relative error is averaged across the trajectories, and is depicted in Figure 6 together with its standard deviation. The prediction error of *N4SID* is the largest, and it grows over time. This is expected, as the method estimates an LTI system without online adaptation. By contrast, the *recursiveLS* algorithm and the proposed method achieve similar performance throughout the test set by successfully adapting the model online. The standard deviation of the prediction error is similar for all methods.

To demonstrate robustness, we introduce a large measurement error in the test data at  $t = 100$ . As shown in Figure 7, the proposed method maintains a significantly smaller average error and standard deviation compared to *recursiveLS*. This aligns with the known robustness of gradient descent algorithms to outliers [47], in contrast to *recursiveLS*, which minimizes the running cost function exactly, and is thus more sensitive to abrupt perturbations.

<sup>3</sup>We note that manually selecting the true order of the system does not improve the predictions for the *N4SID* method.

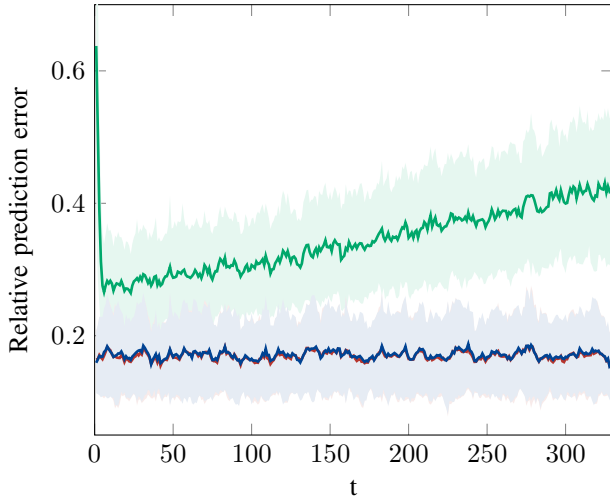


Fig. 6. Relative prediction error of the system models estimated by *N4SID* (green), *recursiveLS* (red), and the proposed method (blue). The solid lines are the average errors across the 100 test trajectories, and the shaded area denotes  $\pm$  one standard deviation.

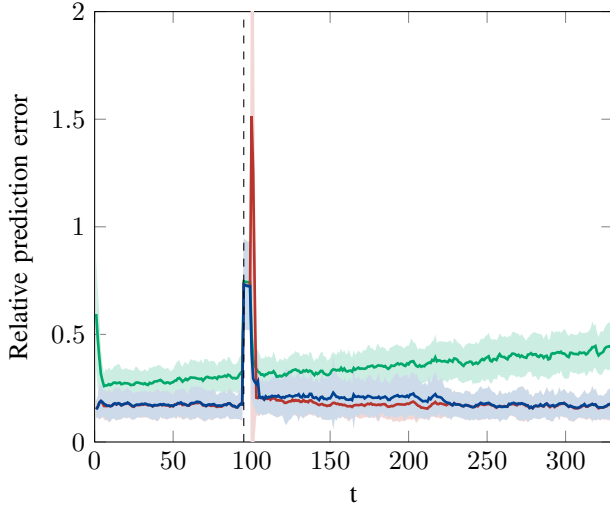


Fig. 7. Relative prediction error of the system models estimated by *N4SID* (green), *recursiveLS* (red), and the proposed method (blue). The solid lines are the average errors across the 100 test trajectories, and the shaded area denotes  $\pm$  one standard deviation. A large measurement error occurs at  $t = 100$  leading to a sudden increase in the error (dashed vertical line). After the large measurement error, the standard deviation of the prediction error produced by the *recursiveLS* method increases to 2.64, and thus, it is not displayed entirely.

## VI. CONCLUSIONS

We proposed an algorithm that tracks time-varying subspaces based on gradient descent on the Grassmannian manifold. Under suitable assumptions on the online data, the uncertainty in the resulting estimates is quantified by an upper bound on their distance to the true subspace. This bound is consistent, in the sense that exponential convergence to a stationary reference subspace is guaranteed in case of noise-free data. The proposed scheme is suitable for online identification of linear time-varying dynamical systems, which is also demonstrated in one of the numerical examples.

Future work includes developing an adaptive data-driven

control framework using the online estimated subspace (c.f., Subspace Predictive Control [40]). Furthermore, the uncertainty quantification of the estimate can be incorporated to robustify the resulting control formulation. Another possible application of the proposed algorithm is fault detection based on the change in system behavior represented by the subspace.

## VII. APPENDIX PROOF OF LEMMA 2

*Proof:* The noisy data matrix can be written as

$$W_t = \underbrace{[\bar{u}_{t-T+1}, \dots, \bar{u}_t]}_{:=\bar{W}_t} + \underbrace{[e_{t-T+1}, \dots, e_t]}_{:=E_t}.$$

Using Lemma 1 and the fact that  $\bar{u}_{t-i} \in \mathbf{U}_{t-i}$  for all  $i = 0, \dots, T-1$ , the projection error of the nominal data in  $\bar{W}_t$  can be bounded as

$$\begin{aligned} \|P_{\mathbf{U}_t}^\perp \bar{W}_t\|_F^2 &= \sum_{i=0}^{T-1} \|P_{\mathbf{U}_t}^\perp \bar{u}_{t-i}\|_2^2 \\ &\leq \sum_{i=0}^{T-1} d_\infty(\mathbf{U}_t, \mathbf{U}_{t-i})^2 \|\bar{u}_{t-i}\|_2^2 \\ &\leq \sum_{i=0}^{T-1} d_2(\mathbf{U}_t, \mathbf{U}_{t-i})^2 \|\bar{u}_{t-i}\|_2^2 \\ &\leq \sum_{i=1}^{T-1} \left( \sum_{k=0}^{i-1} d_2(\mathbf{U}_{t-k}, \mathbf{U}_{t-k-1}) \right)^2 \|\bar{u}_{t-i}\|_2^2 \\ &\leq \sum_{i=0}^{T-1} (ic)^2 \|\bar{u}_{t-i}\|_2^2 = c^2 \|\bar{W}_t D\|_F^2. \end{aligned}$$

Then

$$\begin{aligned} \|P_{\mathbf{U}_t}^\perp W_t\|_F &\leq \|P_{\mathbf{U}_t}^\perp \bar{W}_t\|_F + \|P_{\mathbf{U}_t}^\perp E_t\|_F \\ &\leq c \|\bar{W}_t D\|_F + \|E_t\|_F \\ &\leq c(\|W_t D\|_F + \|E_t D\|_F) + \|E_t\|_F \\ &\leq c\|W_t D\|_F + \|E_t\|_F (c\|D\|_2 + 1). \end{aligned}$$

The claim follows from  $\|E_t\|_F = \sqrt{\sum_{i=0}^{T-1} \|e_{t-i}\|_2^2} \leq \epsilon\sqrt{T}$  and  $\|D\|_2 \leq T-1$ . Note that  $\delta_t$  is strictly monotone, in fact, linear in  $c$  and  $\epsilon$ . ■

## PROOF OF LEMMA 3

In order to prove Lemma 3, we first show that the Riemannian gradient  $\text{grad } d_2(\mathbf{U}, \mathbf{V})^2$  is Lipschitz continuous in the sense of [29, Def. 10.40].

*Lemma 5:* The function  $\text{grad } d_2(\mathbf{U}, \mathbf{V})^2$  on the Grassmannian manifold is  $L$ -Lipschitz continuous in the first argument in the sense of [29, Def. 10.40] with  $L = 4$ .

*Proof:* Note that by [29, Cor. 10.47] the gradient of a twice differentiable function is  $L$ -Lipschitz continuous if and only if its Hessian has operator norm bounded by  $L$ . The Riemannian Hessian of  $d_2(\mathbf{U}, \mathbf{V})^2 = \text{tr}(U^\top P_V^\perp U)$  with respect to the first argument is given as (see [29, Example 9.49, Eq. (9.69)])

$$\text{Hess } d_2(\mathbf{U}, \mathbf{V})[X] = 2P_U^\perp P_V^\perp X - 2XU^\top P_V^\perp U.$$

Note that we use the Frobenius inner product, and hence, the operator norm is defined using the Frobenius norm as

$$\begin{aligned}
\|\text{Hess } d_2(\mathbf{U}, \mathbf{V})\| &= \max_{\substack{X \in \mathcal{T}_{\mathbf{U}}^{\text{Gr}(n,d)} \\ \|X\|_F=1}} \|\text{Hess } d_2(\mathbf{U}, \mathbf{V})[X]\|_F \\
&= \max_{\substack{X \in \mathcal{T}_{\mathbf{U}}^{\text{Gr}(n,d)} \\ \|X\|_F=1}} \|2P_{\mathbf{U}}^\perp P_{\mathbf{V}}^\perp X - 2XU^\top P_{\mathbf{V}}^\perp U\|_F \\
&\leq \max_{\substack{X \in \mathcal{T}_{\mathbf{U}}^{\text{Gr}(n,d)} \\ \|X\|_F=1}} \|2P_{\mathbf{U}}^\perp P_{\mathbf{V}}^\perp X\|_F + \|2XU^\top P_{\mathbf{V}}^\perp U\|_F \\
&\leq \max_{\substack{X \in \mathcal{T}_{\mathbf{U}}^{\text{Gr}(n,d)} \\ \|X\|_F=1}} 2\|P_{\mathbf{U}}^\perp P_{\mathbf{V}}^\perp\|_2 \|X\|_F + 2\|U^\top P_{\mathbf{V}}^\perp U\|_2 \|X\|_F \\
&= 2\|P_{\mathbf{U}}^\perp P_{\mathbf{V}}^\perp\|_2 + 2\|U^\top P_{\mathbf{V}}^\perp U\|_2 \leq 2 + 2\|P_{\mathbf{V}}^\perp U\|_2^2 \\
&\leq 2 + 2\|U\|_2^2 = 4.
\end{aligned}$$

In the following, we provide the proof of Lemma 3 using the result in Lemma 5.

*Proof:* We first exploit the Lipschitzness of  $\text{grad } d_2(\mathbf{U}, \mathbf{V})^2$ , and separate it into a nominal and a noise term in Part I. The nominal part of the gradient contains the signal  $P_{\mathbf{U}_t} W_t$  only, and it is analyzed in Part II. We bound all terms in the gradient that are affected by the noise  $P_{\mathbf{U}_t}^\perp W_t$  in Part III.

**Part I** By Lemma 5, the Riemannian gradient of the squared chordal distance is Lipschitz continuous with constant  $L = 4$ . Therefore, by [29, Cor. 10.54], it holds that

$$\begin{aligned}
d_2(\mathbf{\Gamma}_{k+1}, \mathbf{U}_t)^2 - d_2(\mathbf{\Gamma}_k, \mathbf{U}_t)^2 &\leq -\alpha \langle \text{grad } d_2(\mathbf{\Gamma}_k, \mathbf{U}_t)^2, \text{grad } F_{W_t}(\mathbf{\Gamma}_k) \rangle_F \\
&\quad + 2\alpha^2 \|\text{grad } F_{W_t}(\mathbf{\Gamma}_k)\|_F^2.
\end{aligned} \tag{11}$$

The matrix  $W_t$  can be written as  $W_t = P_{\mathbf{U}_t} W_t + P_{\mathbf{U}_t}^\perp W_t$ . Similarly, we decompose the gradient  $\text{grad } F_{W_t}(\mathbf{\Gamma}_k)$  as  $\text{grad } F_{W_t}(\mathbf{\Gamma}_k) = \bar{G}_t + N_t$ , with

$$\begin{aligned}
\bar{G}_t &:= -2P_{\mathbf{\Gamma}_k}^\perp P_{\mathbf{U}_t} W_t W_t^\top P_{\mathbf{U}_t} \hat{U}, \\
N_t &:= -2P_{\mathbf{\Gamma}_k}^\perp (P_{\mathbf{U}_t}^\perp W_t W_t^\top P_{\mathbf{U}_t}^\perp + P_{\mathbf{U}_t}^\perp W_t W_t^\top P_{\mathbf{U}_t} \\
&\quad + P_{\mathbf{U}_t} W_t W_t^\top P_{\mathbf{U}_t}^\perp) \hat{U}.
\end{aligned}$$

With this partitioning, (11) becomes

$$\begin{aligned}
d_2(\mathbf{\Gamma}_{k+1}, \mathbf{U}_t)^2 - d_2(\mathbf{\Gamma}_k, \mathbf{U}_t)^2 &\leq -\alpha (\langle \text{grad } d_2(\mathbf{\Gamma}_k, \mathbf{U}_t)^2, \bar{G}_t \rangle_F + \langle \text{grad } d_2(\mathbf{\Gamma}_k, \mathbf{U}_t)^2, N_t \rangle_F) \\
&\quad + 2\alpha^2 (\|\bar{G}_t\|_F^2 + 2\langle \bar{G}_t, N_t \rangle_F + \|N_t\|_F^2).
\end{aligned} \tag{12}$$

**Part II** First, we analyze the nominal part of inequality (12). The gradient of the squared chordal distance on the Grassmannian manifold with respect to  $\mathbf{\Gamma}_k$  is  $\text{grad } d_2(\mathbf{\Gamma}_k, \mathbf{U}_t)^2 = -2P_{\mathbf{\Gamma}_k}^\perp P_{\mathbf{U}_t} \hat{U}$ . Furthermore, consider the

compact SVD  $U_t^\top W_t = Q_1 \Sigma Q_2^\top$ . Then

$$\begin{aligned}
&\langle \text{grad } d_2(\mathbf{\Gamma}_k, \mathbf{U}_t)^2, \bar{G}_t \rangle_F \\
&= 4\text{tr}(\hat{U}^\top P_{\mathbf{U}_t} P_{\mathbf{\Gamma}_k}^\perp P_{\mathbf{U}_t} W_t W_t^\top P_{\mathbf{U}_t} \hat{U}) \\
&= 4\text{tr}(U_t^\top P_{\mathbf{\Gamma}_k} P_{\mathbf{U}_t} P_{\mathbf{\Gamma}_k}^\perp U_t U_t^\top W_t W_t^\top U_t) \\
&= 4\text{tr}(Q_1^\top U_t^\top P_{\mathbf{\Gamma}_k} P_{\mathbf{U}_t} P_{\mathbf{\Gamma}_k}^\perp U_t Q_1 \Sigma^2) \\
&\geq \underline{\sigma}^2 4\text{tr}(Q_1^\top U_t^\top P_{\mathbf{\Gamma}_k} P_{\mathbf{U}_t} P_{\mathbf{\Gamma}_k}^\perp U_t Q_1) \\
&= \underline{\sigma}^2 4\text{tr}(\hat{U}^\top P_{\mathbf{U}_t} P_{\mathbf{\Gamma}_k}^\perp P_{\mathbf{U}_t} \hat{U}) = \underline{\sigma}^2 \|\text{grad } d_2(\mathbf{\Gamma}_k, \mathbf{U}_t)^2\|_F^2,
\end{aligned}$$

where we used the fact that  $\Sigma \geq \underline{\sigma} I_d$  by Assumption 3, and

$$\begin{aligned}
&Q_1^\top U_t^\top P_{\mathbf{\Gamma}_k} P_{\mathbf{U}_t} P_{\mathbf{\Gamma}_k}^\perp U_t Q_1 \\
&= Q_1^\top (U_t^\top P_{\mathbf{\Gamma}_k} U_t - U_t^\top P_{\mathbf{\Gamma}_k} P_{\mathbf{U}_t} P_{\mathbf{\Gamma}_k} U_t) Q_1 \\
&= Q_1^\top (U_t^\top P_{\mathbf{\Gamma}_k} I P_{\mathbf{\Gamma}_k} U_t - U_t^\top P_{\mathbf{\Gamma}_k} P_{\mathbf{U}_t} P_{\mathbf{\Gamma}_k} U_t) Q_1 \\
&= Q_1^\top U_t^\top P_{\mathbf{\Gamma}_k} P_{\mathbf{U}_t}^\perp P_{\mathbf{\Gamma}_k} U_t Q_1 \\
&= Q_1^\top U_t^\top P_{\mathbf{\Gamma}_k} P_{\mathbf{U}_t}^\perp P_{\mathbf{U}_t}^\perp P_{\mathbf{\Gamma}_k} U_t Q_1 \geq 0,
\end{aligned}$$

due to the properties of projection matrices. Similarly, the following upper bound holds

$$\begin{aligned}
\|\bar{G}_t\|_F^2 &= 4\text{tr}(\hat{U}^\top P_{\mathbf{U}_t} W_t W_t^\top P_{\mathbf{U}_t} P_{\mathbf{\Gamma}_k}^\perp P_{\mathbf{U}_t} W_t W_t^\top P_{\mathbf{U}_t} \hat{U}) \\
&\leq \bar{\sigma}^2 4\text{tr}(Q_1^\top U_t^\top P_{\mathbf{\Gamma}_k} P_{\mathbf{U}_t} W_t W_t^\top P_{\mathbf{U}_t} P_{\mathbf{\Gamma}_k}^\perp U_t Q_1) \\
&= \bar{\sigma}^2 4\text{tr}(U_t^\top P_{\mathbf{\Gamma}_k}^\perp P_{\mathbf{U}_t} P_{\mathbf{\Gamma}_k} U_t U_t^\top W_t W_t^\top U_t) \\
&\leq \bar{\sigma}^4 4\text{tr}(U_t^\top P_{\mathbf{\Gamma}_k}^\perp P_{\mathbf{U}_t} P_{\mathbf{\Gamma}_k} U_t) \\
&= \bar{\sigma}^4 \|\text{grad } d_2(\mathbf{\Gamma}_k, \mathbf{U}_t)^2\|_F^2.
\end{aligned}$$

**Part III** Now, we bound the terms containing  $N_t$ . The Cauchy-Schwarz inequality yields

$$\begin{aligned}
|\langle \text{grad } d_2(\mathbf{\Gamma}_k, \mathbf{U}_t)^2, N_t \rangle_F| &\leq \|\text{grad } d_2(\mathbf{\Gamma}_k, \mathbf{U}_t)^2\|_F \|N_t\|_F, \\
|\langle \bar{G}_t, N_t \rangle_F| &\leq \|\bar{G}_t\|_F \|N_t\|_F.
\end{aligned}$$

Furthermore,

$$\begin{aligned}
\|\text{grad } d_2(\mathbf{\Gamma}_k, \mathbf{U}_t)^2\|_F &= \|2P_{\mathbf{\Gamma}_k}^\perp P_{\mathbf{U}_t} \hat{U}\|_F \leq \|2P_{\mathbf{\Gamma}_k}^\perp P_{\mathbf{U}_t}\|_F \leq 2r, \\
\|\bar{G}_t\|_F &\leq \bar{\sigma}^2 \|\text{grad } d_2(\mathbf{\Gamma}_k, \mathbf{U}_t)^2\|_F \leq 2r\bar{\sigma}^2.
\end{aligned}$$

Combining the results of Part II and III with (12) yields

$$\begin{aligned}
d_2(\mathbf{\Gamma}_{k+1}, \mathbf{U}_t)^2 - d_2(\mathbf{\Gamma}_k, \mathbf{U}_t)^2 &\leq (-\alpha \underline{\sigma}^2 + 2\alpha^2 \bar{\sigma}^4) \|\text{grad } d_2(\mathbf{\Gamma}_k, \mathbf{U}_t)^2\|_F^2 \\
&\quad + 2\alpha r \|N_t\|_F + 8\alpha^2 r \bar{\sigma}^2 \|N_t\|_F + 2\alpha^2 \|N_t\|_F^2.
\end{aligned}$$

Finally, the triangle inequality and Lemma 2 lead to

$$\begin{aligned}
\|N_t\|_F &\leq 2\|P_{\mathbf{U}_t}^\perp W_t W_t^\top P_{\mathbf{U}_t}^\perp + P_{\mathbf{U}_t}^\perp W_t W_t^\top P_{\mathbf{U}_t} \\
&\quad + P_{\mathbf{U}_t} W_t W_t^\top P_{\mathbf{U}_t}^\perp\|_F \\
&\leq 2\|P_{\mathbf{U}_t}^\perp W_t W_t^\top P_{\mathbf{U}_t}^\perp\|_F + 4\|P_{\mathbf{U}_t} W_t W_t^\top P_{\mathbf{U}_t}^\perp\|_F \\
&\leq 2\|P_{\mathbf{U}_t}^\perp W_t\|_F^2 + 4\|P_{\mathbf{U}_t} W_t\|_2 \|P_{\mathbf{U}_t}^\perp W_t\|_F \\
&\leq 2\delta_t^2 + 4\bar{\sigma}\delta_t.
\end{aligned}$$

Together these yield the right-hand side bound in Lemma 3.  $\blacksquare$

### PROOF OF LEMMA 4

*Proof:* For any  $\mathbf{U}, \tilde{\mathbf{U}} \in \text{Gr}(n, d)$  such that  $\tilde{\mathbf{U}} \in \mathbb{B}_{r_b}(\mathbf{U})$ , the squared chordal distance satisfies the gradient dominance property

$$\begin{aligned} \|\text{grad } d_2(\mathbf{U}, \tilde{\mathbf{U}})\|_F^2 &= 4\text{tr}(P_{\mathbf{U}}P_{\tilde{\mathbf{U}}}P_{\mathbf{U}}^\perp P_{\tilde{\mathbf{U}}}^\perp) \\ &= 4\text{tr}(\tilde{\mathbf{U}}^\top \mathbf{U} \mathbf{U}^\top \tilde{\mathbf{U}} \tilde{\mathbf{U}}^\top P_{\mathbf{U}}^\perp \tilde{\mathbf{U}}) \\ &\geq 4 \min_i \cos^2(\theta_i) \text{tr}(\tilde{\mathbf{U}}^\top P_{\mathbf{U}}^\perp \tilde{\mathbf{U}}) \quad (13) \\ &= 4 \min_i (1 - \sin^2(\theta_i)) d_2(\mathbf{U}, \tilde{\mathbf{U}})^2 \\ &\geq 4(1 - r_b^2) d_2(\mathbf{U}, \tilde{\mathbf{U}})^2, \end{aligned}$$

where  $\theta_i, i = 1, \dots, d$  are the principal angles between  $\mathbf{U}$  and  $\tilde{\mathbf{U}}$ . Therefore, it is sufficient to show that  $\mathbf{\Gamma}_k \in \mathbb{B}_{r_b}(\mathbf{U}_t)$  holds for all  $t \geq T$  and  $k = 0, \dots, K$ .

First, we show by induction that the set  $\mathbb{B}_{r_b}(\mathbf{U}_t)$  is forward invariant under the gradient descent update (7). For a fixed  $t \geq T$ , assume that  $\mathbf{\Gamma}_k \in \mathbb{B}_{r_b}(\mathbf{U}_t)$  for some  $k = 0, \dots, K-1$ . Note that with the choice of  $\alpha$  in Algorithm 1, we have  $\rho > 0$ , and hence,  $\tilde{\rho} < 1$ . Therefore, we can combine the results of Lemma 3 with  $r = r_b$ , and inequality (13) yielding

$$\begin{aligned} d_2(\mathbf{\Gamma}_{k+1}, \mathbf{U}_t)^2 &\leq \tilde{\rho} d_2(\mathbf{\Gamma}_k, \mathbf{U}_t)^2 + \gamma_{r_b}(\delta_t) \\ &\leq \tilde{\rho}^2 r_b^2 + \gamma_{r_b}(\delta_t). \end{aligned}$$

Furthermore, Assumption 4 implies

$$\gamma_{r_b}(\delta_t) \leq (1 - \tilde{\rho}) r_b^2,$$

and therefore,  $\mathbf{\Gamma}_{k+1} \in \mathbb{B}_{r_b}(\mathbf{U}_t)$  holds.

Next, we show that for any  $t \geq T$ ,  $\hat{\mathbf{U}}_{t-1} = \mathbf{\Gamma}_0 \in \mathbb{B}_{r_b}(\mathbf{U}_t)$  implies  $\hat{\mathbf{U}}_t = \mathbf{\Gamma}_K \in \mathbb{B}_{r_b}(\mathbf{U}_{t+1})$ , as illustrated in Figure 3. Due to the invariance of  $\mathbb{B}_{r_b}(\mathbf{U}_t)$  under the gradient descent update (7),  $\mathbf{\Gamma}_k \in \mathbb{B}_{r_b}(\mathbf{U}_t)$  holds at time  $t-1$  for all  $k = 0, \dots, K$ , and hence, inequality (13) applies. We apply the bound in Lemma 3 recursively to get

$$\begin{aligned} d_2(\mathbf{\Gamma}_K, \mathbf{U}_t)^2 &\leq \tilde{\rho}^K d_2(\mathbf{\Gamma}_0, \mathbf{U}_t)^2 + \sum_{k=0}^{K-1} \tilde{\rho}^k \gamma_{r_b}(\delta_t) \\ &\leq \tilde{\rho}^K r_b^2 + \frac{1 - \tilde{\rho}^K}{1 - \tilde{\rho}} \gamma_{r_b}(\delta_t) \leq (r_b - c)^2, \end{aligned} \quad (14)$$

where we used Assumption 4 in the last step. Furthermore, due to the triangle inequality and Assumption 2, we have

$$d_2(\mathbf{\Gamma}_K, \mathbf{U}_{t+1}) \leq d_2(\mathbf{\Gamma}_K, \mathbf{U}_t) + d_2(\mathbf{U}_t, \mathbf{U}_{t+1}) \leq r_b,$$

which completes the proof.  $\blacksquare$

### PROOF OF THEOREM 1

*Proof:* From the proof of Lemma 4, we have

$$d_2(\hat{\mathbf{U}}_t, \mathbf{U}_t)^2 \leq \tilde{\rho}^K d_2(\hat{\mathbf{U}}_{t-1}, \mathbf{U}_t)^2 + \frac{1 - \tilde{\rho}^K}{1 - \tilde{\rho}} \gamma_{r_b}(\delta_t).$$

Therefore, the following bound holds for any  $t \geq T$

$$\begin{aligned} d_2(\hat{\mathbf{U}}_t, \mathbf{U}_t)^2 &\leq \tilde{\rho}^K d_2(\hat{\mathbf{U}}_{t-1}, \mathbf{U}_t)^2 + \frac{1 - \tilde{\rho}^K}{1 - \tilde{\rho}} \gamma_{r_b}(\|\delta\|_\infty) \\ &\leq \tilde{\rho}^K (d_2(\hat{\mathbf{U}}_{t-1}, \mathbf{U}_{t-1}) + c)^2 \\ &\quad + \frac{1 - \tilde{\rho}^K}{1 - \tilde{\rho}} \gamma_{r_b}(\|\delta\|_\infty) \\ &\leq \tilde{\rho}^K d_2(\hat{\mathbf{U}}_{t-1}, \mathbf{U}_{t-1})^2 + \tilde{\rho}^K (2r_b - c)c \\ &\quad + \frac{1 - \tilde{\rho}^K}{1 - \tilde{\rho}} \gamma_{r_b}(\|\delta\|_\infty), \end{aligned}$$

where we used the facts that  $d_2(\hat{\mathbf{U}}_{t-1}, \mathbf{U}_{t-1}) \leq r_b - c$  from inequality (14), and  $\gamma_{r_b}(\delta_t) \leq \gamma_{r_b}(\|\delta\|_\infty)$  for any  $t \geq T$ . We apply the above inequality recursively leading to

$$\begin{aligned} d_2(\hat{\mathbf{U}}_t, \mathbf{U}_t)^2 &\leq \tilde{\rho}^{Kt} d_2(\hat{\mathbf{U}}_0, \mathbf{U}_0)^2 \\ &\quad + \sum_{\tau=0}^{t-1} (\tilde{\rho}^K)^\tau \left( \frac{1 - \tilde{\rho}^K}{1 - \tilde{\rho}} \gamma_{r_b}(\|\delta\|_\infty) + \tilde{\rho}^K (2r_b - c)c \right). \end{aligned}$$

Substituting the solution of the geometric series completes the proof.  $\blacksquare$

- [1] J. Coulson, J. Lygeros, and F. Dörfler, "Data-enabled predictive control: In the shallows of the DeePC," in *18th European Control Conference*, pp. 307–312, IEEE, 2019.
- [2] J. Coulson, J. Lygeros, and F. Dörfler, "Distributionally robust chance constrained data-enabled predictive control," *IEEE Transactions on Automatic Control*, vol. 67, no. 7, pp. 3289–3304, 2021.
- [3] J. Berberich, J. Köhler, M. A. Müller, and F. Allgöwer, "Data-driven model predictive control with stability and robustness guarantees," *IEEE Transactions on Automatic Control*, vol. 66, no. 4, pp. 1702–1717, 2020.
- [4] V. Breschi, A. Chiuso, and S. Formentin, "Data-driven predictive control in a stochastic setting: A unified framework," *Automatica*, vol. 152, p. 110961, 2023.
- [5] J. C. Willems, P. Rapisarda, I. Markovskiy, and B. L. De Moor, "A note on persistency of excitation," *Systems & Control Letters*, vol. 54, no. 4, pp. 325–329, 2005.
- [6] C. Verhoek, H. S. Abbas, R. Tóth, and S. Haesaert, "Data-driven predictive control for linear parameter-varying systems," in *Proc. 4th IFAC Workshop on Linear Parameter Varying Systems LPVS*, vol. 54, pp. 101–108, Elsevier, 2021.
- [7] H. J. van Waarde, J. Eising, H. L. Trentelman, and M. K. Camlibel, "Data informativity: A new perspective on data-driven analysis and control," *IEEE Transactions on Automatic Control*, vol. 65, no. 11, pp. 4753–4768, 2020.
- [8] C. De Persis and P. Tesi, "Formulas for data-driven control: Stabilization, optimality, and robustness," *IEEE Transactions on Automatic Control*, vol. 65, no. 3, pp. 909–924, 2019.
- [9] J. C. Willems and J. W. Polderman, *Introduction to mathematical systems theory: A behavioral approach*, vol. 26. Springer Science & Business Media, 1997.
- [10] I. Markovskiy and F. Dörfler, "Identifiability in the behavioral setting," *IEEE Transactions on Automatic Control*, vol. 68, no. 3, pp. 1667–1677, 2023.
- [11] P. Van Overschee and B. De Moor, *Subspace identification for linear systems: Theory, implementation, applications*. Boston: Kluwer, 1996.
- [12] F. Dörfler, P. Tesi, and C. De Persis, "On the Certainty-Equivalence Approach to Direct Data-Driven LQR Design," *IEEE Transactions on Automatic Control*, vol. 68, no. 12, pp. 7989–7996, 2023.
- [13] I. Markovskiy and F. Dörfler, "Behavioral systems theory in data-driven analysis, signal processing, and control," *Annual Reviews in Control*, vol. 52, pp. 42–64, 2021.
- [14] J. Berberich and F. Allgöwer, "An overview of systems-theoretic guarantees in data-driven model predictive control," *Annual Review of Control, Robotics, and Autonomous Systems*, vol. 8, 2025.
- [15] C. Verhoek, P. J. Koelewijn, S. Haesaert, and R. Tóth, "Direct data-driven state-feedback control of general nonlinear systems," *arXiv preprint arXiv:2303.10648*, 2023.

- [16] J. Berberich, J. Köhler, M. A. Müller, and F. Allgöwer, “Linear tracking MPC for nonlinear systems—Part II: The data-driven case,” *IEEE Transactions on Automatic Control*, vol. 67, no. 9, pp. 4406–4421, 2022.
- [17] J.-P. Delmas, “Subspace tracking for signal processing,” in *Adaptive signal processing: next generation solutions*, pp. 211–270, Wiley-IEEE Press, 2010.
- [18] N. V. Dung, N. L. Trung, and K. Abed-Meraim, “Robust subspace tracking algorithms in signal processing: A brief survey,” *REV Journal on Electronics and Communications*, vol. 11, no. 1-2, 2021.
- [19] L. Balzano, Y. Chi, and Y. M. Lu, “Streaming PCA and Subspace Tracking: The Missing Data Case,” *Proceedings of the IEEE*, vol. 106, no. 8, pp. 1293–1310, 2018.
- [20] J. R. Bunch and C. P. Nielsen, “Updating the singular value decomposition,” *Numerische Mathematik*, vol. 31, no. 2, pp. 111–129, 1978.
- [21] B. Yang, “Projection approximation subspace tracking,” *IEEE Transactions on Signal Processing*, vol. 43, pp. 95–107, 1995.
- [22] J. He, L. Balzano, and A. Szlam, “Incremental gradient on the grassmannian for online foreground and background separation in subsampled video,” in *IEEE Conference on Computer Vision and Pattern Recognition*, pp. 1568–1575, 2012.
- [23] L. Balzano, R. Nowak, and B. Recht, “Online identification and tracking of subspaces from highly incomplete information,” in *48th Annual Allerton Conference on Communication, Control, and Computing (Allerton)*, pp. 704–711, 2010.
- [24] J. Xu, V. K. Ithapu, L. Mukherjee, J. M. Rehg, and V. Singh, “GOSUS: Grassmannian online subspace updates with structured-sparsity,” in *Proc. IEEE International Conference on Computer Vision*, pp. 3376–3383, 2013.
- [25] N. Vaswani, T. Bouwmans, S. Javed, and P. Narayanamurthy, “Robust subspace learning: Robust PCA, robust subspace tracking, and robust subspace recovery,” *IEEE Signal Processing Magazine*, vol. 35, no. 4, pp. 32–55, 2018.
- [26] N. Vaswani and P. Narayanamurthy, “Finite sample guarantees for PCA in non-isotropic and data-dependent noise,” in *55th Annual Allerton Conference on Communication, Control, and Computing (Allerton)*, pp. 783–789, IEEE, 2017.
- [27] D. Zhang and L. Balzano, “Global convergence of a grassmannian gradient descent algorithm for subspace estimation,” in *Proc. 19th International Conference on Artificial Intelligence and Statistics*, pp. 1460–1468, 2016.
- [28] A. Edelman, T. A. Arias, and S. T. Smith, “The geometry of algorithms with orthogonality constraints,” *SIAM Journal on Matrix Analysis and Applications*, vol. 20, no. 2, pp. 303–353, 1998.
- [29] N. Boumal, *An introduction to optimization on smooth manifolds*. Cambridge University Press, 2023.
- [30] P.-A. Absil, R. Mahony, and R. Sepulchre, *Optimization Algorithms on Matrix Manifolds*. Princeton: Princeton University Press, 2008.
- [31] S. Boyd and L. Vandenberghe, *Convex optimization*. Cambridge university press, 2004.
- [32] P. Van Overschee and B. De Moor, “N4SID: Subspace algorithms for the identification of combined deterministic-stochastic systems,” *Automatica*, vol. 30, no. 1, pp. 75–93, 1994.
- [33] L. Ljung, *System identification theory for the user*. Upper Saddle River, NJ, USA: Prentice-Hall, 1999.
- [34] G. H. Golub and C. F. Van Loan, *Matrix computations*. Baltimore, MD, USA: Johns Hopkins Univ. Press, 2013.
- [35] R. A. Horn and C. R. Johnson, *Matrix analysis*. Cambridge university press, 2012.
- [36] K. Ye and L.-H. Lim, “Schubert varieties and distances between subspaces of different dimensions,” *SIAM Journal on Matrix Analysis and Applications*, vol. 37, no. 3, pp. 1176–1197, 2016.
- [37] A. Padoan, J. Coulson, H. J. Van Waarde, J. Lygeros, and F. Dörfler, “Behavioral uncertainty quantification for data-driven control,” in *IEEE 61st Conference on Decision and Control*, pp. 4726–4731, IEEE, 2022.
- [38] W. J. Rugh, *Linear system theory*. Englewood Cliffs, NJ, USA: Prentice-Hall, 1996.
- [39] P.-Å. Wedin, “Perturbation bounds in connection with singular value decomposition,” *BIT Numerical Mathematics*, vol. 12, pp. 99–111, 1972.
- [40] W. Favoreel, B. De Moor, and M. Gevers, “SPC: Subspace predictive control,” *IFAC Proceedings Volumes*, vol. 32, no. 2, pp. 4004–4009, 1999.
- [41] J. Coulson, H. J. Van Waarde, J. Lygeros, and F. Dörfler, “A quantitative notion of persistency of excitation and the robust fundamental lemma,” *IEEE Control Systems Letters*, vol. 7, pp. 1243–1248, 2022.
- [42] J. Berberich, A. Iannelli, A. Padoan, J. Coulson, F. Dörfler, and F. Allgöwer, “A quantitative and constructive proof of Willems’ fundamental lemma and its implications,” in *American Control Conference*, pp. 4155–4160, IEEE, 2023.
- [43] F. Zhao, F. Dörfler, A. Chiuso, and K. You, “Data-enabled policy optimization for direct adaptive learning of the LQR,” *arXiv preprint arXiv:2401.14871*, 2024.
- [44] E. Sontag, “Smooth stabilization implies coprime factorization,” *IEEE Transactions on Automatic Control*, vol. 34, no. 4, pp. 435–443, 1989.
- [45] K. Åström and B. Wittenmark, *Adaptive Control*. Dover Books on Electrical Engineering, Dover Publications, 2008.
- [46] N. Boumal, B. Mishra, P.-A. Absil, and R. Sepulchre, “Manopt, a Matlab toolbox for optimization on manifolds,” *Journal of Machine Learning Research*, vol. 15, no. 42, pp. 1455–1459, 2014.
- [47] A. Ali, E. Dobriban, and R. Tibshirani, “The implicit regularization of stochastic gradient flow for least squares,” in *Proc. 37th International Conference on Machine Learning*, vol. 119, pp. 233–244, 2020.